A COMBINED EXPERIMENTAL-NUMERICAL STUDY TO CYCLIC BEHAVIOUR OF LIMESTONE

K. De Proft[*], G.N. Wells[†], L.J. Sluys[†] and W.P. De Wilde[*]

[*] Department of Mechanics of Materials and Constructions
Vrije Universiteit Brussel
Pleinlaan 2, 1050 Brussel, Belgium.
e-mail: kurt.deproft@vub.ac.be

[†] Faculty of Civil Engineering and Geosciences
Delft University of Technology
Stevinweg 1, 2628 CN, Delft, The Netherlands
Email: L.J.Sluys@citg.tudelft.nl

Key words: cohesive zone, damage-plasticity, partition of unity, ESPI

Abstract. *In this paper, a combined experimental-computational study of double-edge notched stone specimen subject to cyclic tensile loading is presented. In the experimental part, the load-deformation response and the local displacement field are recorded. Both experimental results are used to validate a numerical model for the description of fracture within finite elements. The model uses displacement discontinuities to model cracks. These discontinuities are implemented using the partition of unity property of finite element shape functions. In the discontinuity, a combined damage-plasticity cohesive law is used. Numerical simulations are compared with experimental observations.*

1

1 INTRODUCTION

Currently, a variety of computational techniques exist to describe fracture of quasi-brittle materials. These numerical models must be able to simulate the behaviour of brittle materials for different loading conditions. Therefore, experimental data is very important. Firstly, experimental data is needed in order to determine whether the proposed numerical models are capable of simulating the observed behaviour. Secondly, experimental data are also necessary to obtain a certain number of model parameters included in the numerical model. Conversely, numerical models can also be used to improve the experimental design.

Obviously, the link between experiments and computational tools is extremely important. In this paper, a combined experimental-computational study of double-edge notched (DEN) stone specimens, subjected to cyclic tensile loading is presented. In the first section, the experimental set-up is presented and discussed. This is followed by a discussion of the experimental results. Both global, *i.e.* load-deformation response, as well as local, *i.e.* displacement field around the crack tip, information is recorded. Then, cohesive zone model is used to model the DEN tests. A combined damage-plasticity cohesive zone law is adopted. In the final section, numerical results are compared with experimental values.

2 EXPERIMENTAL SET-UP

For the experiments, a natural stone called 'Massangis' is used. All specimens are 120 mm high and 50 mm wide. The thickness is 11 mm. Notches 7 mm deep and 1 mm wide are sawn in the middle of both sides of the specimen. The geometry of the specimen is shown in figure 1. Two Linear Variable Differential Transducers (LVDT) are used for the measurement of the deformation. The LVDT's are placed over the notches on each side of the specimen, as indicated in figure 1. The vertical measuring range of the LVDT's is 20 mm. Due to the notches, the crack will be located within the range of the LVDT's. When a macro crack starts to grow, the deformations tend to localize in the cracked area. Other parts of the specimen will unload. When the crack is not in the range of the LVDT's or when the measuring range of the LVDT's is too large, a snap back will occur making the measurement of the post peak behaviour impossible. In the other case, when the crack is situated in the range of the LVDT's, the measured deformation increases gradually. The average signal of the LVDT's can then be used as the control signal for the test. The average signal is also used in the load-deformation curves.

The experiments are performed with an INSTRON 4505 testing bench. The specimens are directly glued to the loading platens, so that the boundaries of the specimen cannot rotate. Tensile loading is applied by a uniform vertical displacement of the boundary. In the post peak, two unloading-reloading sequences are carried out. All tests were performed under displacement control at a rate of 0.3 μm/s.
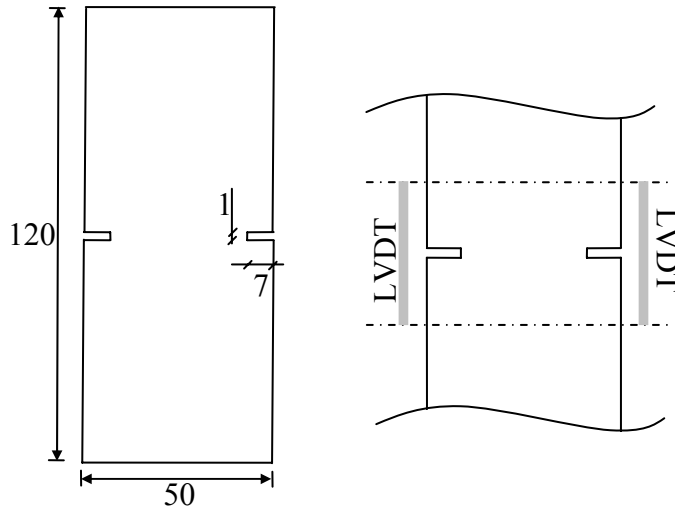
Figure 1 : Geometry of the specimen (all dimensions in mm) and placement of LVDT.

An ESPI (Electronic Speckle Pattern Interferometer) device is used to record the local displacement field at different load steps. The specimen is illuminated by laser light and speckles appear on the lighted surface. A CCD camera captures the reflected light. The observed speckle pattern includes information about the deformation of the specimen. By subtracting different speckle patterns, interference fringes are formed. These fringes contain information about the displacement of the studied specimen. Unlike strain gauges, there is no contact with the studied specimen and the strain field, which can be computed with the software, of a section of the specimen can be studied. A user-defined border restricts the measuring area of the ESPI. Within this border, a reference point is defined. This reference point is assumed not to move and the displacements of all material points situated inside the border are referred to the reference point. In order to compare with numerical results, five paths are defined along which the displacements are monitored at several load steps. The different load paths and the position of the reference point are shown in figure 2. Subtracting the displacements along path 1 from the displacements along path 2 results in the deformation between those two paths.

3   EXPERIMENTAL RESULTS

A typical load-deformation curve is shown in figure 3. Examining the load-deformation curve, three issues should be emphasized:

- After complete unloading, the closure of the crack is not complete.
- The unloading stiffness reduces with increasing deformation.
- During the unloading/reloading cycle, a small amount of energy is dissipated.
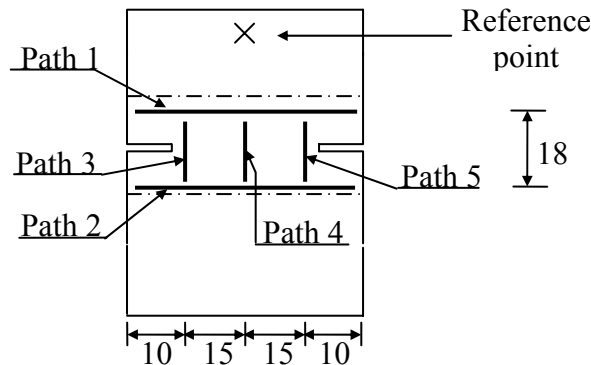
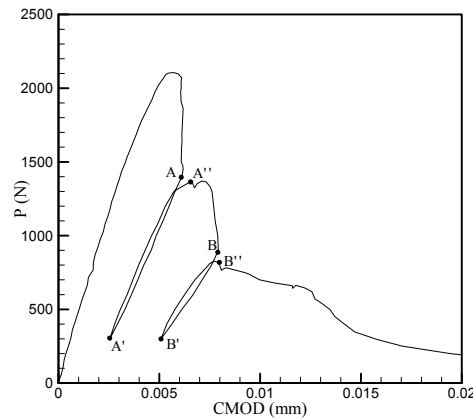Figure 2: Position of the reference point and paths for ESPI measurement.

Figure 3: Load-deformation curve for cyclic loaded specimen.

Black dots represent points where a snapshot of the displacement field is taken. The deformations δ between path 1 and path 2 are computed and are shown in figure 4. The deformations before (A) and after (A') unloading and after reloading (A") are given in figure 4a. It is clear that before unloading (A), a crack is growing from the right notch. The deformations are highly non-uniform. Then, the tensile loading is decreased until *P = 300N*. When the deformations obtained after unloading are studied (A'), it is clear that the specimen is divided into two parts:

a) A first part where deformations are vanishing when the load is decreasing, indicating elastic or damage behaviour.

b) A second part where, after unloading, permanent deformations occur.

After reloading (A"), the deformations recover to approximately the same values as before unloading. The loading-unloading-reloading cycle is repeated further in the post peak branch. Examining the deformations in figure 4b, the same conclusions can be drawn. Notice that the permanent deformations after unloading have increased, compared with the first cycle.
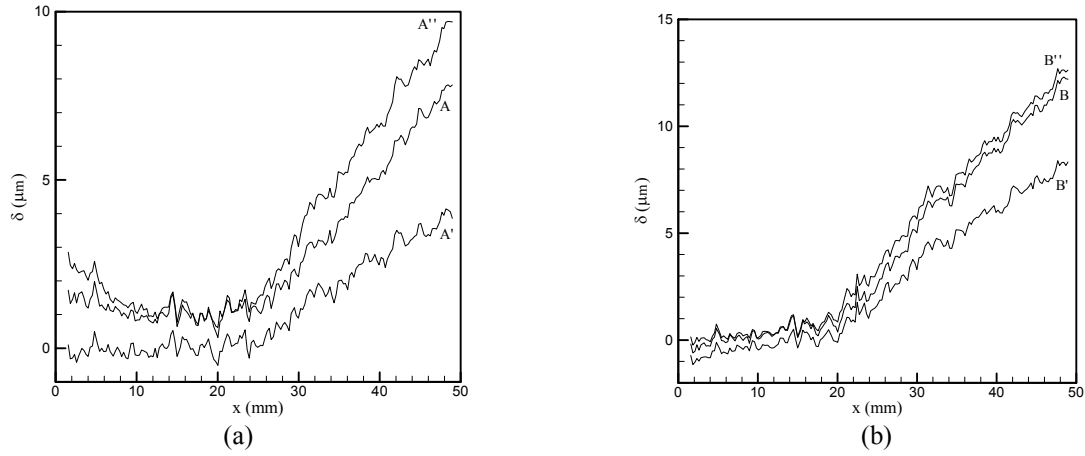
Figure 4: Deformations before and after unloading and after reloading for (a) the first cycle and (b) the second cycle.
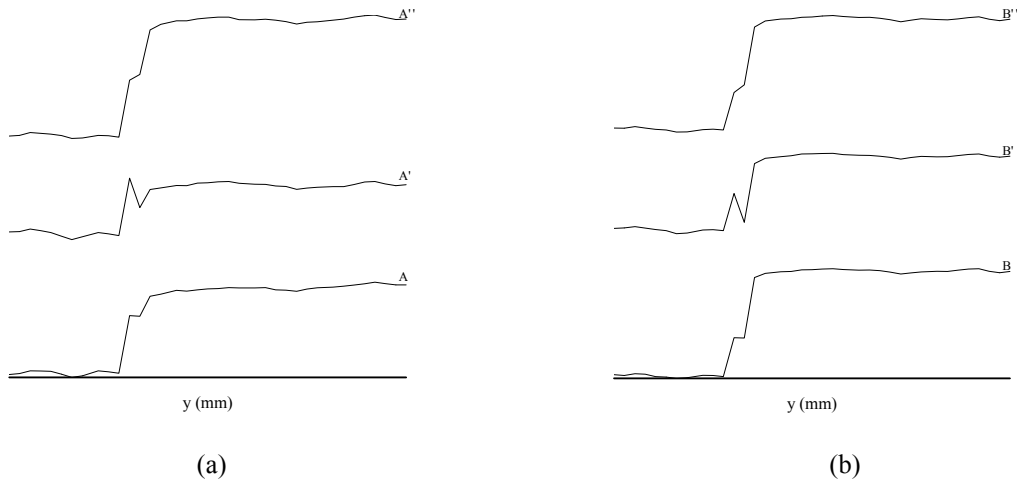

Figure 5: Evolution of displacements along path 5 for (a) first cycle and (b) the second cycle.

Displacements along path 5 are shown in figure 5. The represented values refer to the reference point and are only used for an indication of the evolution of the displacement jumps. From figure 5, it is clear that after unloading the crack does not completely close.

4 NUMERICAL MODEL

The experimental results, presented in the previous section, are now compared with numerical simulations. Cracks are modelled as displacement discontinuities. The displacement field of a body crossed by *m* non-intersecting discontinuities is given by

$$\mathbf{u} = \hat{\mathbf{u}} + \sum_{i=1}^{m} H_{\Gamma_i} \widetilde{\mathbf{u}}_i \tag{1}$$

where $\hat{\mathbf{u}}$ and $\widetilde{\mathbf{u}}$ are continuous functions and $H_{\Gamma i}$ is the Heaviside step function. The infinitesimal strain field can be found by taking the symmetric gradient of the displacement

field:

$$\mathbf{\varepsilon} = \nabla^s \hat{\mathbf{u}} + \sum_{i=1}^{m} H_{\Gamma_i} \nabla^s \tilde{\mathbf{u}}_i + \sum_{i=1}^{m} \delta_{\Gamma_i} \left(\tilde{\mathbf{u}}_i \otimes \mathbf{n} \right)^s \qquad (2)$$

where $\mathbf{n}$ is the normal to the discontinuity and $\delta_{\Gamma i}$ is the Dirac delta distribution. The displacement field is implemented within the finite element context using the partition of unity property of the finite element shape functions. When a crack crosses a finite element, nodes are locally enhanced by additional degrees of freedom with the Heaviside step function as an enhancement basis[i,ii].

Making use of the partition of unity property, the displacement field is obtained by:

$$\mathbf{u} = \mathbf{N}\mathbf{a} + \sum_{i=1}^{m} H_{\Gamma_i} \mathbf{N}\mathbf{b}_i \qquad (3)$$

where $\mathbf{N}$ are the finite element shape functions, $\mathbf{a}$ are the regular degrees of freedom, $\mathbf{b}$ are the enhanced degrees of freedom and m is the number of non-intersecting cracks. The governing finite element equations[iii] can be obtained as:

$$\begin{bmatrix} \mathbf{K}_{aa} & \mathbf{K}_{ab_1} & \cdots & \mathbf{K}_{ab_m} \\ \mathbf{K}_{b_1 a} & \mathbf{K}_{b_1 b_1} & \cdots & \mathbf{K}_{b_1 b_m} \\ \vdots & \vdots & \vdots & \vdots \\ \mathbf{K}_{b_m a} & \mathbf{K}_{b_m b_1} & \cdots & \mathbf{K}_{b_m b_m} \end{bmatrix} \begin{Bmatrix} d\mathbf{a} \\ d\mathbf{b}_1 \\ \vdots \\ d\mathbf{b}_m \end{Bmatrix} = \begin{Bmatrix} \mathbf{f}_a^{ext,t+\Delta t} \\ 0 \\ \vdots \\ 0 \end{Bmatrix} - \begin{Bmatrix} \mathbf{f}_a^{int,t} \\ \mathbf{f}_{b_1}^{int,t} \\ \vdots \\ \mathbf{f}_{b_m}^{int,t} \end{Bmatrix} \qquad (4)$$

where

$$\mathbf{K}_{aa} = \int_{\Omega} \mathbf{B}^T \mathbf{C}^e \mathbf{B} d\Omega$$

$$\mathbf{K}_{ab_j} = \int_{\Omega} H_{\Gamma_j} \mathbf{B}^T \mathbf{C}^e \mathbf{B} d\Omega$$

$$\mathbf{K}_{ab_j} = \int_{\Omega} H_{\Gamma_j} \mathbf{B}^T \mathbf{C}^e \mathbf{B} d\Omega \qquad (5)$$

$$\mathbf{K}_{b_i b_j} = \int_{\Omega} H_{\Gamma_i} H_{\Gamma_j} \mathbf{B}^T \mathbf{C}^e \mathbf{B} d\Omega$$

$$\mathbf{K}_{b_j b_j} = \int_{\Omega} H_{\Gamma_j} \mathbf{B}^T \mathbf{C}^e \mathbf{B} d\Omega + \int_{\Gamma_j} \mathbf{N}^T \mathbf{D} \mathbf{N} d\Gamma_j$$

where $\mathbf{C}^e$ is the continuum elastic material tensor, $\mathbf{D}$ is the material tangent for the discontinuity. It is assumed that the considered element is crossed by discontinuity j and influenced by discontinuity i.

The continuum is assumed to remain elastic, while the behaviour in the discontinuity is inelastic. From the experimental study, it became obvious that the observed behaviour is a

combination of damage and plasticity (see figure 3). Consequently, the behaviour in the discontinuity is described by a combined damage-plasticity model. The discrete material model is derived from the continuum case where a combination of damage and plasticity can be obtained by writing[iii,iv,v]:

$$\boldsymbol{\sigma} = (1-d)\mathbf{C}^e\left(\boldsymbol{\varepsilon} - \boldsymbol{\varepsilon}^{pl}\right) \tag{6}$$

where $\boldsymbol{\sigma}$ is the stress tensor, d is a damage variable, $\boldsymbol{\varepsilon}$ is the total strain tensor and $\boldsymbol{\varepsilon}^{pl}$ is the plastic strain tensor. The damage is governed by a damage loading function, given by:

$$f^d = \varepsilon^{eq} - \kappa^d \tag{7}$$

where ε^{eq} is the equivalent strain measure and κ^d is the history parameter. The equivalent strain is defined as:

$$\varepsilon^{eq} = \sqrt{\sum_{i=1}^{3} \langle \varepsilon_i \rangle^2} \tag{8}$$

where $\langle \varepsilon_i \rangle = \left(\varepsilon_i + |\varepsilon_i|\right)/2$ and ε_i is the i-th principal strain. The history parameter κ^d represents the most severe value of equivalent strain measure ever reached. When the damage grows, the damage variable is updated via:

$$d = 1 - \frac{q(\kappa^d)}{\kappa^d} = 1 - \frac{\kappa_i \exp\left[-\beta\kappa^d\right]}{\kappa^d} \tag{9}$$

where κ_i is the damage threshold. Plastic deformations are assumed to occur in the undamaged material bonds, so that the plastic yield function can be expressed in the effective stress space,

$$f^p = \phi(\hat{\boldsymbol{\sigma}}) - \overline{\sigma}(\kappa^p) \tag{10}$$

where $\hat{\boldsymbol{\sigma}}$ is the effective stress tensor, defined as:

$$\hat{\boldsymbol{\sigma}} = \frac{\boldsymbol{\sigma}}{1-d} \tag{11}$$

and κ^p is the internal plastic variable. Introducing the effective stress tensor in equation (6) reduces to the classical elasto-plastic problem:

$$\hat{\boldsymbol{\sigma}} = \mathbf{C}^e\left(\boldsymbol{\varepsilon} - \boldsymbol{\varepsilon}^p\right) \tag{12}$$

The plastic strain rate is defined according to the classical flow theory of plasticity,

$$\dot{\boldsymbol{\varepsilon}}^p = \dot{\lambda}\frac{\partial f}{\partial \hat{\boldsymbol{\sigma}}} \tag{13}$$

where λ is the plastic multiplier.

The combined damage-plasticity model is given in terms of stress and strains. In order to be useful in equation 4, the model must be redefined in terms of tractions and separations. Therefore, the expression for the strain field, given in equation (2) is inserted in equation (6):

$$\boldsymbol{\sigma} = (1-d)\mathbf{C}^e\left(\nabla^s\hat{\mathbf{u}} + H_{\Gamma_i}\nabla^s\tilde{\mathbf{u}} + \delta_{\Gamma_i}(\tilde{\mathbf{u}}\otimes\mathbf{n})^s - \boldsymbol{\varepsilon}^{pl}\right) \tag{14}$$

Assuming that the plastic strain field can be decomposed in a similar form as the total strain field and that the damage variable κ^d ($\kappa^d = \overset{=d}{\kappa} + \delta_{\Gamma_i}\overline{\kappa}^d$) has a distributed character[vi], equation (14) can be rewritten,

$$\boldsymbol{\sigma}_P = \frac{q(\overline{\kappa}^d)}{\overline{\kappa}^d}\mathbf{C}^e\left((\tilde{\mathbf{u}}\otimes\mathbf{n})^s - (\tilde{\mathbf{u}}^{pl}\otimes\mathbf{n})^s\right) \tag{15}$$

where 'p' stands for a point on the discontinuity. In equation (15), plasticity and damage is only allowed at the discontinuity. From equation (15), the tractions can be obtained as;

$$\mathbf{t} = \frac{q(\overline{\kappa}^d)}{\overline{\kappa}^d}\mathbf{n}\mathbf{C}^e\mathbf{n}\left(\boldsymbol{\Delta} - \boldsymbol{\Delta}^{pl}\right) = (1-\omega)\mathbf{Q}^e\left(\boldsymbol{\Delta} - \boldsymbol{\Delta}^{pl}\right) \tag{16}$$

where ω is the degenerated damage variable and $\mathbf{Q}^e$ is the elastic acoustic tensor. Examining equation (16), a significant similarity with the continuum model is observed. A major difference is that the elastic part has disappeared in the degenerated model, so that the separation of the discontinuity is completely inelastic. The total separation at the discontinuity is split into a recoverable damage part and an irrecoverable plastic part. Furthermore, the elastic constitutive tensor is replaced by the elastic acoustic tensor. Finally, the continuum damage variable d is replaced by the degenerated damage variable ω, which varies between –infinity and 1. The evolution of the degenerated damage variable is governed by the degenerated internal variable $\overline{\kappa}^d$, which represents the most severe value of an equivalent strain measure ever reached. The equivalent strain measure is given in terms of strains and needs to be rewritten in terms of separations. The equivalent strain measure, given in equation (8), can be easily degenerated as:

$$\Delta^{eq} = \Delta_n \tag{17}$$

where Δ^{eq} is the equivalent discontinuity separation and Δ_n is the normal separation of the discontinuity.

The damage function can be rewritten as:

$$f^d = \Delta^{eq} - \overline{\kappa}^d \tag{18}$$

and the degenerated damage variable is found as

$$\omega = 1 - \frac{q(\overline{\kappa}^d)}{\overline{\kappa}^d} = 1 - \frac{\kappa_i}{\kappa^d}\exp\left[-\beta\overline{\kappa}^d\right] \tag{19}$$

The plastic yield function is written in terms of tractions,

$$f^p = \hat{T}_n - (H\kappa^p) \tag{20}$$

where $\hat{T}_n$ is the effective normal traction, H is the softening modulus and κ^p is the internal plastic variable.

5   NUMERICAL SIMULATIONS VS EXPERIMENTAL RESULTS

In this section, the numerical model (cohesive zone model with a combined damage-plasticity cohesive law) is used to simulate the DEN tensile tests. The deformation profiles, shown in figure 4, clearly showed that non-symmetric crack growth occurred during the tests. The numerical model, presented in previous section, should be enriched in order to capture this non-symmetric crack growth. Two types of enrichment can be taken into account: (i) local weakening of the material at one notch or (ii) introduction of a bending component. Both types are further explored.
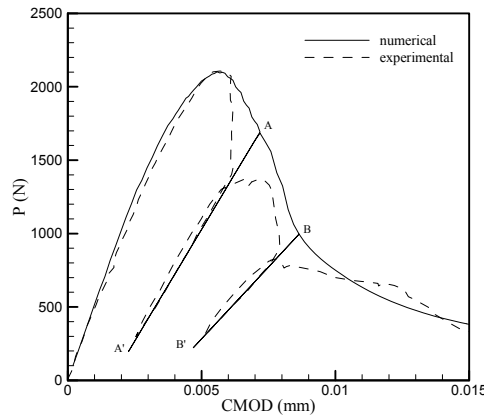

Figure 6: Comparison of experimental and numerical (with material weakness) obtained load-deformation curve for cyclic loading.

Figure 6 compares the experimental load-deformation curve with the simulated curve using an imperfection at the right notch. The adopted model parameters are: f_t = 6.5 MPa, h = 27000 N/mm^3 and β = 400. Clearly, the peak load is captured correctly. Also the decrease of the stiffness and the appearance of permanent deformations are captured in a correct way. The computed deformation profiles are compared with the experimental profiles in figure 7. For unloading branch 1, the deformation profiles are similar. After unloading (figure 7.b), the calculation shows permanent deformations at the left side of the specimen, while the experimental deformations largely disappear. This means that during the calculation, a discontinuity is already introduced at the left side, while in reality, the behaviour is still elastic.   For the second unloading branch (figure 7.d), the difference is even more pronounced.

The same simulations are repeated for non-symmetric crack growth triggered by an additional bending moment. The load is applied with a small eccentricity. The value of the eccentricity is e = 2.2 mm. The adopted model parameters are: f_t = 7.8 MPa, h = 27000 N/mm^3 and β = 400. The obtained load-deformation curve and the deformation profiles are shown in

figure 8 and figure 9 respectively. The computed global response is in good agreement with the measured response. Obviously, the experimental profiles are better captured when a bending component is introduced. Furthermore, the computed deformations are higher than the measured ones.
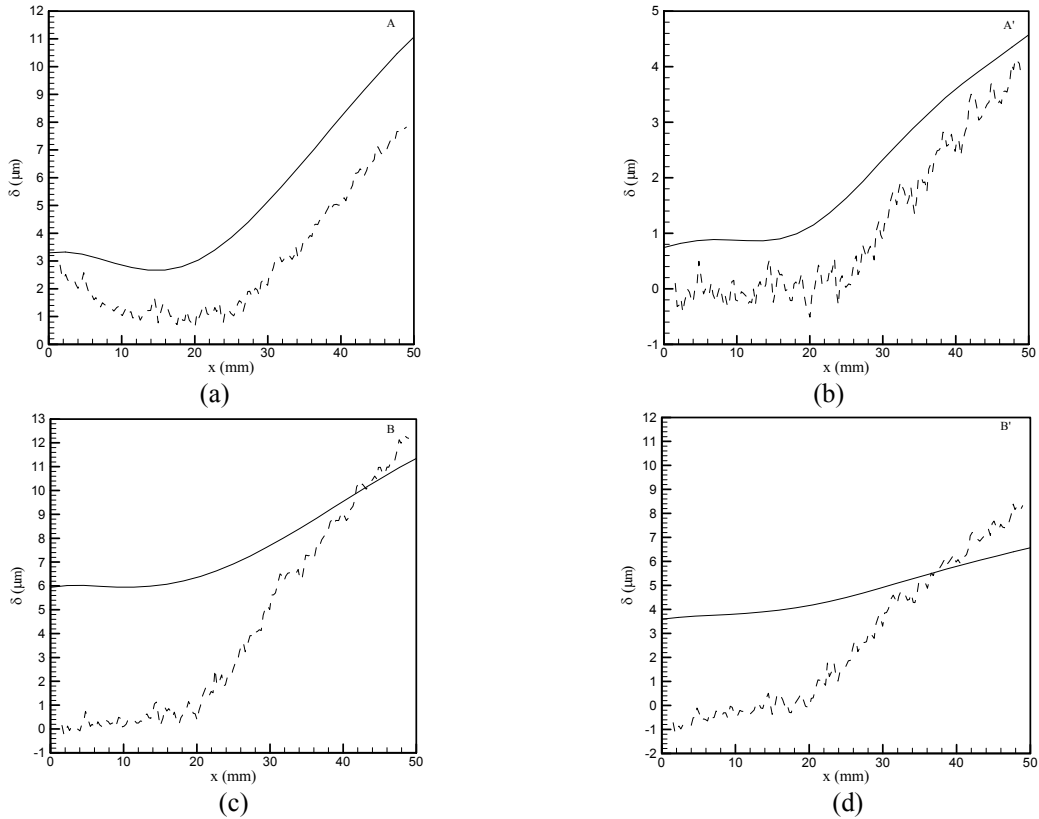

(a)

(b)

(c)

(d)

Figure 7: Deformation profiles for (a) begin and (b) end unloading branch 1 and (c) begin and (d) end unloading branch 2.
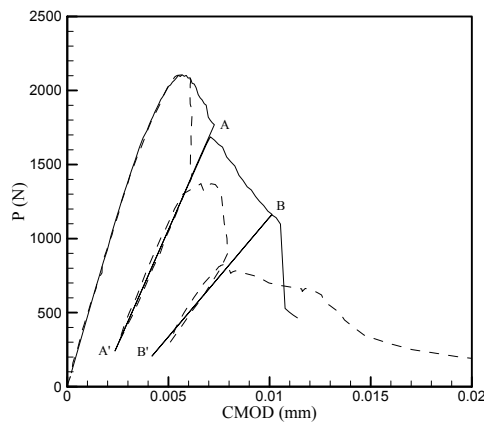

Figure 8: Comparison of experimental and numerical (with added bending) obtained load-deformation curve for cyclic loading.
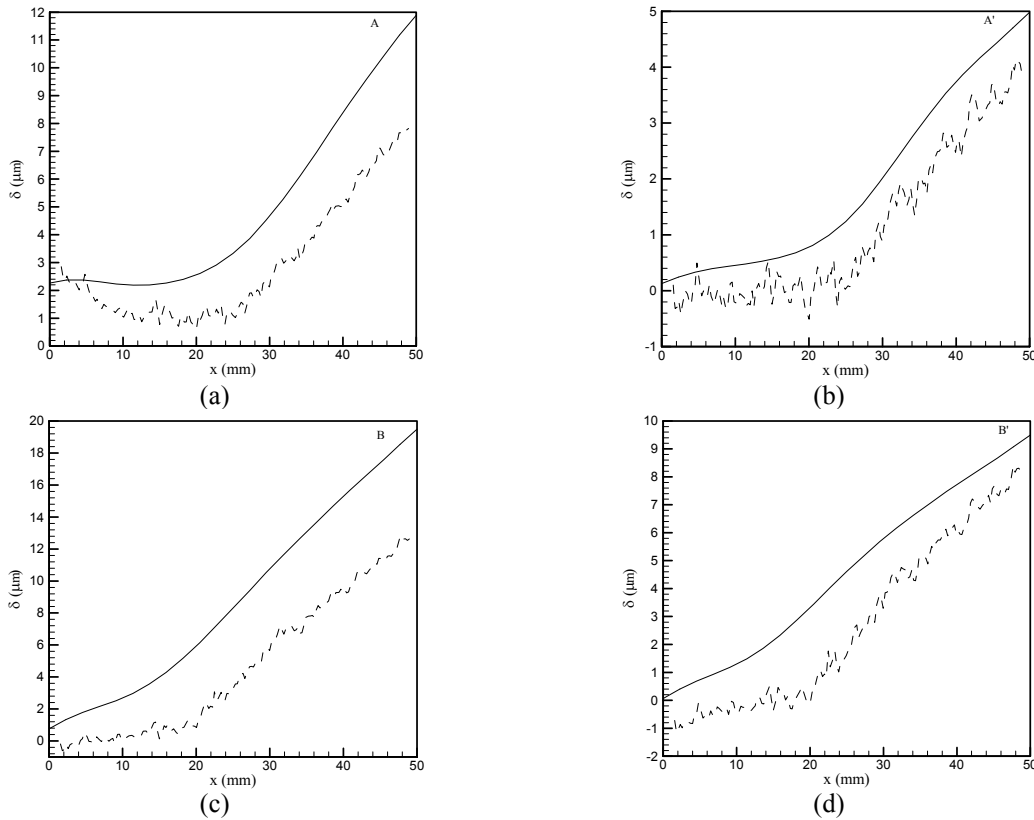
Figure 9: Deformation profiles for (a) begin and (b) end unloading branch 1 and (c) begin and (d) end unloading branch 2.

6 CONCLUSIONS

In this paper, a combined experimental-computational study of cyclic behaviour of limestone is presented. During the experiment, both global and local measurements were performed. Globally, the load-deformation curve was recorded. When unloading, a decrease of stiffness and permanent deformations were observed. Locally, the displacement field around the crack tip was measured. It was shown that the use of the ESPI technique gives important extra information. Measurements showed that the obtained deformations are non-symmetric. Moreover, the ESPI is very useful since there is no contact with the specimen, and consequently, the measurement is not interfered.

For the numerical simulations, the cohesive zone model based on partition of unity was used in combination with a damage-plasticity model. In order to correctly describe the experiments, the model must be enhanced. Therefore, a weaker region or an additional bending component was added. It was shown that adding bending resulted in the best agreement with the experiments.

Obviously, the result shows that the comparison of numerical simulations with experimental

data should be carried out with great care. A fit of the simulations to the global data is not sufficient to conclude that the adopted model can capture the material behaviour.

7. ACKNOWLEDGEMENTS

REFERENCES

[i]   G.N. Wells and L.J. Sluys, "A new method for modelling cohesive cracks using finite elements", *Int. J. Num. Meth. Eng.*, **50**(12), 2667-2682 (2001).

[ii] Moës N., Dolbow J. and Belytschko T., "A finite element method for crack growth without remeshing", *Int. J. Num. Meth. Eng*, **46**, 131-150 (1999).

[iii] K. De Proft, "A combined experimental-computational study to discrete fracture of brittle materials" , Phd thesis, Vrije Universiteit Brussel, (2003).

[iv] Simo J.C. and Ju, J.W., "Strain- and stress-based continuum damage models – I. Formulation", *International Journal of Solids and Structures,* **23**(7), 821-840 (1987).

[v]   Simo J.C. and Ju, J.W., "Strain- and stress-based continuum damage models – II. Computational aspects", *International Journal of Solids and Structures,* **23**(7), 841-869 (1987).

[vi] Oliver, J., "On the discrete constitutive models induced by strong discontinuity kinematics and continuum constitutive equations", *International Journal of Solids and Structures,* **37**, 7207-7229 (2000).